Available online at www.sciencedirect.com

ScienceDirect

Procedia Manufacturing 34 (2019) 101–109

Procedia MANUFACTURING

www.elsevier.com/locate/procedia

47th SME North American Manufacturing Research Conference, Penn State Behrend Erie, Pennsylvania, 2019

Ultrasonic Vibration Turning to Increase the Deposition Efficiency of a silica-based Sol-Gel Coating

R. Bertolini[a]*, S. Bruschi[a], A. Ghiotti[a], L. Pezzato[a]

[a]*Dept. of Industrial Engineering, University of Padova, Via Venezia 1, 35131, Padova, Italy*

* Corresponding author. Tel.: +39 049 8276819; fax: +39 049 8276819. *E-mail address:* rachele.bertolini@phd.unipd.it

Abstract

Magnesium alloys are attracting more and more attention for producing temporary prosthetic devices thanks to their bioresorbable characteristics in human environment. However, they present a reduced corrosion resistance to body fluids, which still limits their applications to a great extent. One possible way to increase the corrosion performances is to coat the device with a suitable coating that provides a barrier to the body fluids corrosion. In this work, Ultrasonic Vibration Turning (UVT) is used to create a surface texture to the AZ31 magnesium alloy with the aim of improving the surface wettability and therefore helping the subsequent coating deposition. The obtained results showed that the surface texture induced by UVT contributed to increase the surface wettability of approximately 17% compared to the conventional turning case, regardless of the adopted cutting parameters. The UVT texture proved to improve the efficiency of the coating deposition since the thickness of the deposited sol-gel coating was increased when applied to UVT surfaces, especially at the lowest depth of cut and highest cutting speed that contributed to generate deeper dimples.

Keywords: Magnesium Alloy; Ultrasonic Vibration; Turning; Texture; Coating

1. Introduction

Magnesium and its alloys have attracted much attention as bioresorbable implant materials thanks to their biocompatibility and biodegradability [1]. However, their fast degradation when placed in the human environment limits their practical application to a great extent [2]. Different approaches have been developed to improve the durability of magnesium alloys, such as element alloying [3], mechanical treatments [4][5], and coatings [6].

Different types of coatings were attempted to improve the magnesium alloys corrosion resistance, especially the organic-base ones since they offer protection against corrosion but at the same time they can be functionalized with organic biomolecules [6]. Among these, the sol–gel technique is a simple method for applying various coatings to a broad range of materials, especially in case of parts characterized by complex geometries, involving the immersion of the substrate into a liquid medium [7]. In order to have an efficient deposition of the coating, the substrate must present adequate wettability characteristics.

To this regard, Ultrasonic Vibration Turning (UVT) can represent a promising method to modify the wettability of surfaces while machining them at the same time. As example, Elliptical Vibration Cutting (EVC) was used in [8], as a mean to realize two-level hierarchical microstructures capable to modify the anisotropy of the water droplet, namely the difference between the contact angles measured in the parallel and perpendicular directions. Controllable sinusoidal micro-textures with a wavelength of one order of magnitude smaller than the widths of the first-order micro-channels were formed on the surface in order to modify the isotropy of the water droplet. In this way, super hydrophobic surfaces were created. In [9] the same technology was applied for generating

10.1016/j.promfg.2019.06.126

different micro-textures on aluminum cylinders. Micro-dimples, micro-channels, and grid patterns were obtained by carefully choosing the process parameters, showing that the dimple patterns overall increased the surface hydrophobicity compared to the one of the smooth pre-machined cylinders. Moreover, besides the dimples texture, the feed increase was proved to decrease the area fraction of the solid-liquid contact, which, according to the Cassie-Baxter model, decreases the water droplet contact angle. In addition, the controversial effect of the depth of cut was proved, since, above a certain level, dimples overlapped each other. When the depth of cut was set smaller than a critical value, the dimples shape determined the surface topography. In this situation, the area fraction of the solid-liquid contact increased at increasing depth of cut, and therefore, the water droplet contact angle increased at the same time. On the contrary, when the depth of cut was larger than the critical value, micro-channels began to form, whose width and depth increased at increasing depth of cut.

Feed-direction Ultrasonic Vibration-Assisted Turning (FUVAT) was used to generate micro-textured surface on copper 1100 in [10]. The effect of several parameters including amplitude, feed rate, and spindle speed on patterns and shapes of the obtained microstructures was investigated. It was found that, compared with the surface fabricated by turning without ultrasonic vibration, the hydrophilicity of the textured surfaces was enhanced.

However, in none of the aforementioned studies UVT was used as a mean to improve the efficiency of a coating deposition thanks to the wettability increase of the machined surfaces. To this regard, UVT is here used as a way to machine magnesium surfaces with a unique patterned surface texture for a subsequent coating deposition. Surfaces with different dimples geometries, which can act as puddles for the coating solution, were produced through UVT, then a sol-gel coating was deposited and its characteristics evaluated.

2. Experimental

2.1. Material

The material under investigation is the commercially available AZ31 magnesium alloy. In order to homogenize the initial microstructure, the material was first subjected to an annealing heat treatment at 360°C for 2 hours followed by air cooling. Fig. 1 shows the obtained microstructure.

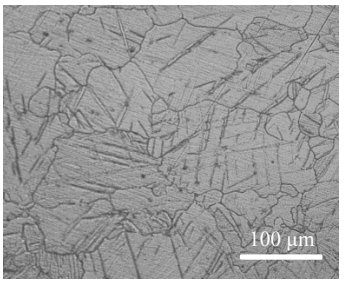

Fig. 1. Microstructure of the AZ31 magnesium alloy after the annealing heat treatment.

2.2 Machining trials

The machining trials were performed on a Mori Seiki™ NL 1500 CNC lathe equipped with an UVT apparatus. Fig. 2a shows schematically the UVT process. The workpiece rotates along the X-axis at a constant cutting speed (*Vc*), while the cutting tool moves at a constant feed (*f*) along the same axis, called hereafter “feed direction”. The tool vibrates at ultrasonic frequency along the Y axis, called hereafter “vibration direction”. Fig. 2b shows the overall experimental equipment, mounted on the lathe.

The UVT system refers to the set of the piezoelectric transducer, the sonotrode, the tool tip, and the mechanical setup to fit in the turret of the lathe. More details about the experimental apparatus can be found in [11].

The used turning insert was a VCEX110301LF1125 with a radius of 0.1 mm supplied by Sandvik Coromant™.

Samples were prepared through two subsequent stages: the first consisted in a conventional turning pass, while the second was a finishing pass at a constant feed of 0.05 mm/rev. The second pass was carried out using two different approaches, namely Conventional Turning (CT) and UVT. Two different values of the cutting speed, namely 100 m/min and 200 m/min, and depth of cut, namely 0.05 mm and 0.01 mm, were adopted. The vibration frequency, equal to 30 kHz, was kept fixed for all the tests. The tests were performed under dry conditions and repeated five times for each cutting parameter.

Table 1 summarizes the experimental plan adopted for the machining trials.

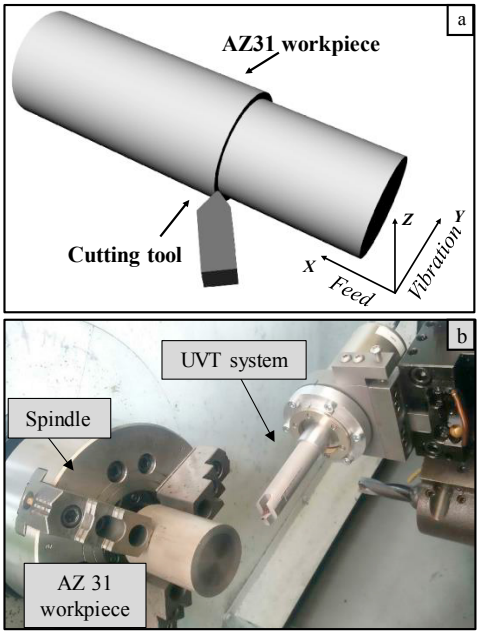

Fig. 2. a) Scheme of the UVT process; b) UVT experimental setup mounted on the lathe.

Table 1. Experimental plan for the machining trials.

Test ID	Turning approach	Depth of Cut *DoC* (mm)	Cutting speed *Vc* (m/min)
S1	CT	0.05	100
S2	UVT	0.05	100
S3	CT	0.05	200
S4	UVT	0.05	200
S5	CT	0.1	100
S6	UVT	0.1	100
S7	CT	0.1	200
S8	UVT	0.1	200

2.3 Microstructural and mechanical characterization

After machining, the AZ31 cylinders were cut to prepare metallographic samples. The samples were cold mounted, ground using up to 4000 SiC grit paper, and then polished using 3 μm diamond paper and SiO_2 colloidal dispersion in demineralized water. The polished samples were cleaned in an acetone ultrasound bath for 15 min, then rinsed in demineralized water, and finally dried by compressed air. Acetic and picric acid aqueous solution was used as etchant to reveal the grain boundaries. The microstructure observations were conducted using a Leica™ DMRE optical microscope equipped with a high definition digital camera.

Measurements of nano-hardness were carried out by means of the iMicro™ nano-indenter from Nanomechanics Inc. making use of a Berkovich diamond indenter. Indentations were performed with a load of 25 mN along a line composed by six points, starting from approximately a distance of 50 μm from the machined surface.

The load was kept low enough in order to minimize the distance between two subsequent points and, thus, allow appreciating differences between the samples. Measurements were performed on three different zones across the section of each sample.

2.4 Surface topography analysis

The surface topography of the AZ31 machined cylinders was inspected using a Sensofar™ PLU-Neox optical profiler with a 20x Nikon™ confocal objective.

Data processing, filtering and evaluation of the surface texture parameters were performed according to the ISO 25178 series.

A number of surface textures parameters were evaluated on the basis of previous research studies on wettability [12], but only the ones relevant to the purpose of this study are here reported:

- Arithmetical mean height of the scale-limited surface (*Sa*), the most popular areal parameter, which represents the baseline for comparison with other research works.
- Reduced dale height (*Svk*), a parameter effective in discriminating the presence of dimples generated by the ultrasonic motion of the tool.
- Reduced peak height (*Spk*), a parameter giving information about the height of the surface top portions that influence the support of the liquid droplet.
- Skewness of the scale-limited surface (*Ssk*), which refers to the symmetry of the profile about the mean line. Similarly to *Spk*, it influences the contact area between the surface and the water droplet.
- Kurtosis of the scale-limited surface (*Sku*), which is a measure of the sharpness of the roughness profile.

Besides the aforementioned surface texture parameters, an additional indicator was taken into account, namely the Aspect Ratio (*AR*) of the dimples, which refers to the ratio between the dimples depth and mean diameter.

The dimples average depth was calculated on the basis of three measurements of depth taken on the 2D profile, which was extracted from the 3D topography of the machined surface at six fixed coordinates. Three different topographies were considered for such calculation for each cutting condition.

The dimples diameter d_{gap} (μm) is considered equal to the distance between two subsequent dimples and can be expressed through Eq. (1):

$$d_{gap} = 10^6 \frac{V_c}{60f} \quad (1)$$

where *Vc* (m/min) is the cutting speed and *f* (Hz) the ultrasonic frequency.

The mapping of the machined surface defects was performed using the optical profiler with the 20X confocal objective.

For each sample, three sampling areas of 4000 μm of length and 700 μm of height were analyzed. The nature of the different surface defects was assessed with the help of the 2D profiles.

2.5 Contact angle measurement

The measure of the contact angle to evaluate the wettability of the AZ31 machined cylinders was carried out applying a static sessile drop technique. The experimental apparatus is schematically reported in Fig. 3. Basically, it consisted of a micrometer syringe to form a liquid drop, a halogen and intensity adjustable light source to illuminate the sample, and a Prosilica GT™ camera for the images acquisition. Before measuring, the samples were cleaned in an ultrasound bath for 15 min to remove any residue.

A liquid droplet of distilled water of 10 μL of volume was used and let fall on the lateral surface of the cylindrical sample. The measurements were conducted at room temperature (25°C), repeated eight times for each machining condition to assure reproducibility, and the mean value was finally calculated.

Top view images of the droplets fallen on the cylindrical samples were also acquired by means of the optical profiler with a 10x Nikon™ confocal objective.

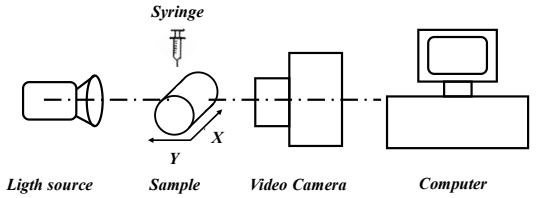

Fig. 3. Scheme of the wettability measurement setup.

2.6 Coating deposition

A modified silica-based sol-gel coating was deposited on the surfaces turned with and without ultrasonic vibration in order to verify the suitability of ultrasonic vibration to produce a surface that could guarantee good characteristics for the sol-gel deposition. The reagents used to produce the sol-gel coating were methyl-triethoxy-silane (MTES, 99%), tetraethyl orthosilicate (TEOS, 98%), ethanol, hydrochloric acid (1N), and distilled water.

The sol-gel silica coating solutions were synthetized under acidic conditions: ethanol, silica precursors, water and then hydrochloric acid were added in a beaker under vigorous stirring in a molar ratio of 2:1:4:0.01, respectively. The ratio between TEOS and MTES was fixed at 30:70.

After 30 minutes, the sol-gel was deposited by dip coating on CT and UVT samples with a withdraw speed of 4.8 cm/min. Afterwards, the samples were heat treated (curing step) inside a furnace at 250°C for 1 hour, and slowly cooled down into the furnace.

2.7 Coating characterization

A Zeiss™ Stemi C-2000 stereo microscope was used to acquire images of the sample surface before and after coating.

In addition, the coating thickness was evaluated on the basis of the procedure reported below. After being coated, the samples were cut. Then, a gold layer was deposited on their surface to protect it from the polishing steps. The gold deposition was performed using a POLARON™ SEM coating system working at 2.4 KV for 60 s. After that, the samples were cold mounted in resin, ground and polished with the same procedure described in Section 2.3.

The Cambridge Stereoscan™ 440 Scanning Electron Microscope (SEM), equipped with a Philips™ PV9800 EDS working in backscattered electron mode, was used to examine the coated surfaces and images at 5000X of magnification were acquired in different zones of the samples.

On these images, thickness measurements were performed using the ImageJ™ software every 20 μm.

3. Results and discussion

3.1 Microstructural and mechanical characterization of the machined workpieces

The optical micrographs reported in Fig. 4 on the left show the presence of a thin sub-surface layer characterized by heavily deformed grains along the cutting direction just under the machined surface. The thickness of such layer appears not to be significantly influenced by the turning approach, even if in CT samples the layer resulted to be more homogeneous.

Fig. 4 on the right reports the nano-hardness values as a function of the distance from the machined surface for CT and UVT samples machined using a depth of cut of 0.05 mm.

The absence of significant hardness changes confirms what evidenced by the optical microscopy images, namely the absence of any microstructure changes in terms of size or phases. Besides that, no significant nano-hardness differences between the CT and UVT samples were found.

The same conclusions were achieved in [13], in which UVT was applied to a titanium alloy and no sensible differences in hardness were found between the bulk and the UVT processed material.

3.2 Topography analysis of the machined surfaces

Fig. 5 shows the textures of the S1 and S2 samples that differ just for the turning approach. As expected, the surface topography of the S2 sample machined using ultrasonic vibration is extremely different from that of the CT sample.

The UVT sample surface looks symmetrical, thanks to the presence of a grid characterized by convex and concave features. This is indicative of the fact that during machining the cutting tool vibrated with a certain amplitude at ultrasonic frequency inducing an intermittent contact with the workpiece.

Table 2 reports the values of the surface texture parameters as a function of the different cutting parameters.

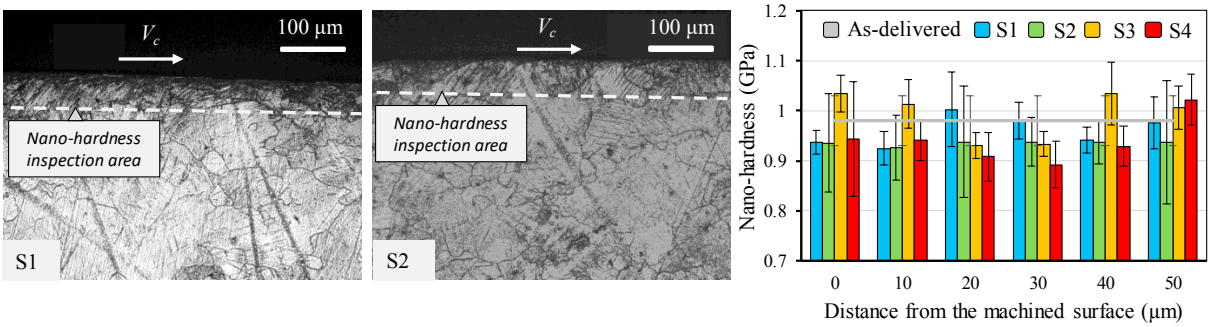

Fig. 4. Microstructures of (a) the S1 and (b) the S2 samples on the left. Nano-hardness of the CT and UVT samples machined using a depth of cut of 0.05 mm on the right (see test ID in Table 1)

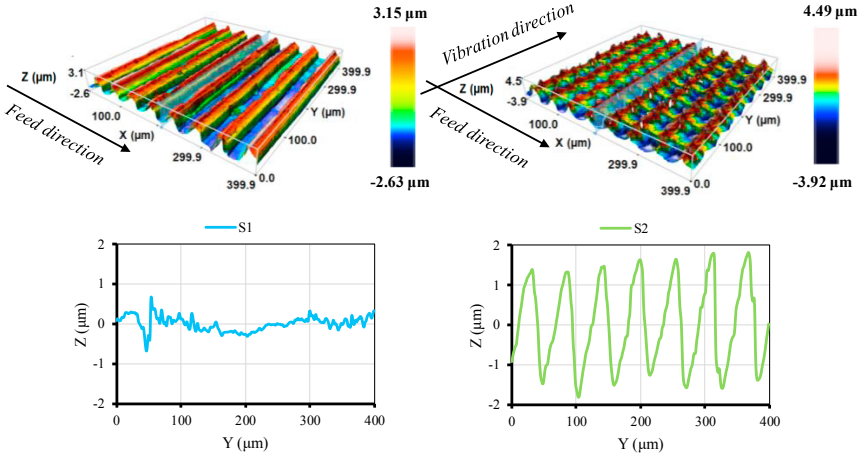

Fig. 5. 3D topographies and relative 2D profiles of the S1 (left) and S2 (right) samples.

Sa is one of the most popular surface area parameters and still the one used for sake of comparison between different studies. Two different situations can be identified: at the lowest depth of cut, a clear trend could not be found, while, when a depth of cut equal to 0.1 mm was applied, UVT led to a sensible reduction of *Sa*, regardless of the adopted cutting speed. The *Sa* reduction achieved a maximum of 43% in the case of S6 sample compared to the S5 one. This can be attributed to the fact that, contrary to the UVT approach, the cutting tool and the workpiece are always in contact when applying CT: the use of severe cutting parameters may induce the generation of defects, such as thick, uneven and severe cracked chips, built-up edge, as well as the development of high cutting forces, frictional heat, and high-cutting instability, which may deteriorate the machined surface and finally produce a rougher surface [14]. On the contrary, UVT is characterized by reduced cutting forces, frictional forces and frictional heat, produces sharper and finer chips that have less influence on the machined surface thanks to the limited contact between the tool and the workpiece [14].

The functional height 3D parameters are related to the heights and depth of peaks and valleys, and they have a significant impact on the lubrication and contact performances of the machined surface. Again, a clear trend could be identified only in the case of the highest depth of cut. Actually, a reduction of these parameters is obtained by the introduction of the ultrasonic motion of the tool, regardless of the adopted cutting speed. These data are in accordance with the *Sa* reduction.

From these evidences, it can be postulated that, among the investigated ones, the depth of cut is the cutting parameter that mostly influences the surface roughness profile. Actually, since the depth of cut determines the amount of material removed during cutting, its effect is coupled with the one given by the amplitude of vibration: such synergistic effect provokes the aforementioned differences in the roughness profiles.

Lastly, both *Ssk* and *Sku* did not evidence any clear trend as a consequence of the introduction of the ultrasonic vibration.

The geometric characteristics of the dimples induced by UVT can be modified by changing the cutting parameters. Table 3 reports the AR measurements while Fig. 6 displays partial 2D profiles of different UVT samples. By increasing the cutting speed from 100 m/min to 200 m/min, the dimples pattern becomes sparser along the vibration direction, as predicted by Eq. 1. In addition, from the upper part of Fig. 6, it can be seen that the cutting speed did not substantially modify the size and shape of the dimples, in the case of the lowest depth of cut, while, on the contrary, it contributed to the generation of different dimples shapes in the case of the highest depth of cut. As a consequence of that, a clear trend of the dimples AR with the cutting speed cannot be identified.

On the contrary, the depth of cut influenced the dimples AR in an unambiguous way (see Table 3): at increasing depth of cut, the dimples AR decreased, namely they became larger and shorter.

Table 2. Areal surface texture parameters. Relative standard deviations: Sa < 10%, Spk < 10%, Sku < 15%, Ssk < 10%, Spk < 10% and Svk < 10%

	Sa (µm)	Ssk (-)	Sku (-)	Spk (µm)	Svk (µm)
S1	1.15	0.05	3.49	1.49	0.55
S2	1.11	0.12	2.62	1.22	1.08
S3	0.97	0.33	2.92	0.78	1.37
S4	1.28	0.08	2.46	1.13	0.96
S5	1.17	0.07	2.47	0.92	0.66
S6	0.67	0.35	2.9	0.73	0.39
S7	1.17	0.14	3.18	1.29	0.94
S8	0.74	0.13	2.67	0.85	0.64

Table 3. Average depth, average length and AR of the UVT induced dimples (see test ID in Table 1).

Test ID	Average depth (µm)	Average length (µm)	AR
S2	3.1 ± 0.3	55	0.06
S4	4.4 ± 0.2	111	0.04
S6	0.6 ± 0.3	55	0.01
S8	2.1 ± 0.3	111	0.02

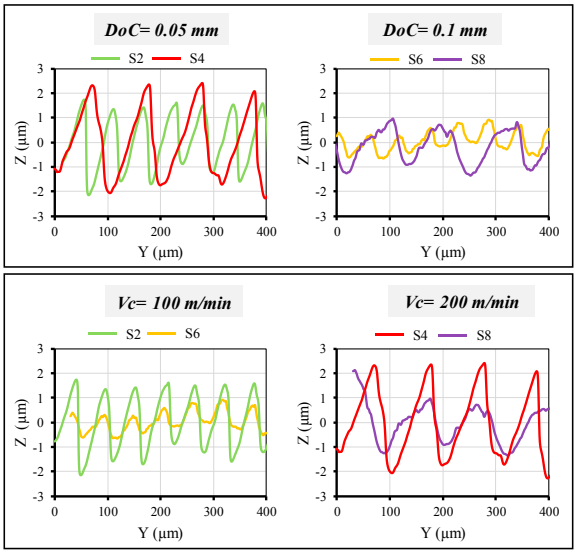

Fig. 6. Comparison between different profiles along the vibration direction.

Therefore, it can be stated that the depth of cut has an important influence on the pattern arrangement along the vibration direction. The lower part of Fig. 6 clearly shows these evidences.

These experimental data are in accordance with the surface roughness results, which indicate that a depth of cut increase leads to a sensible reduction of both *Spk* and *Svk*, therefore inducing the formation of stubbier peaks.

3.3 Machined surface defects

The main defects found on the surface of the samples machined using CT and UVT are shown in Fig. 7 using red circles. The analysis of the machined surface defects is mandatory, since they can affect the coating adhesion.

In general, it can be seen that UVT promoted a lower formation of surface defects. The presence of surface defects was emphasized by the adoption of more severe process parameters regardless of the turning approach.

The S3 sample presents in fact feed marks irregularities, tearing and particles, whereas the S4 sample shows a defects free surface. The same defects that characterize the S3 sample are present on the S5 one, even if in the latter case they are larger and denser. On the contrary, just signs of feed marks irregularities appear on the S6 sample.

The reason of the lower presence of defects on the UVT sample surfaces can be again ascribed to the intermittent contact between the cutting tool and the workpiece when machining using ultrasonic vibration: this induces lower cutting forces and temperatures, smaller chips that are easily carried away from the cutting zone, which, in turn, produces a more uniform surface [15].

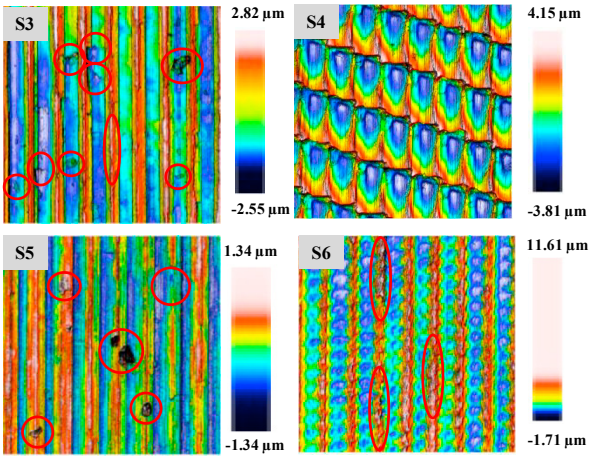

Fig. 7. Defects on the machined surfaces (see test ID in Table 1).

Similarly, the adoption of more severe process parameters led to an increase of the cutting forces and temperatures promoting the formation of defects, also in the case of UVT, even if to a less extent.

It is worth noting that the depth of cut has the major influence compared to the cutting speed in forming defects as can be seen also from Fig. 6 where the profiles obtained at the highest depth of cut appear much more jagged.

3.4 Wettability characteristics

Water droplet contact angles on the surfaces made by CT (S1 sample) and UVT (S2 sample) are reported in Fig. 8. Similar outcomes were found for the other cutting conditions and, therefore, are not here reported.

As can be seen, UVT contributed to increase wettability by lowering the contact angle. The wettability increase is of about 17% compared to the CT samples, regardless of the adopted cutting parameters.

The top view of the droplet shows that the droplet assumes a more isotropic configuration in the case of UVT surfaces, covering in a more homogenous way the surface along the cutting direction. The shape of the water droplet is symmetric along the feed and vibration directions, while in the case of CT it is elongated along the feed direction. This means that UVT contributes to the formation of a more isotropic surface, since the water droplet tends to remain spherical, without deforming along a preferential direction [8].

Wettability behaviour mainly depends on two factors, namely the surface energy that, in turn, depends on both surface chemical composition and mechanical characteristics of the surface, and the surface topography [16]. Materials characterized by high surface energy are more hydrophilic (as their surface needs more energy to break molecular bonds between the surface and the liquid in contact) [17].

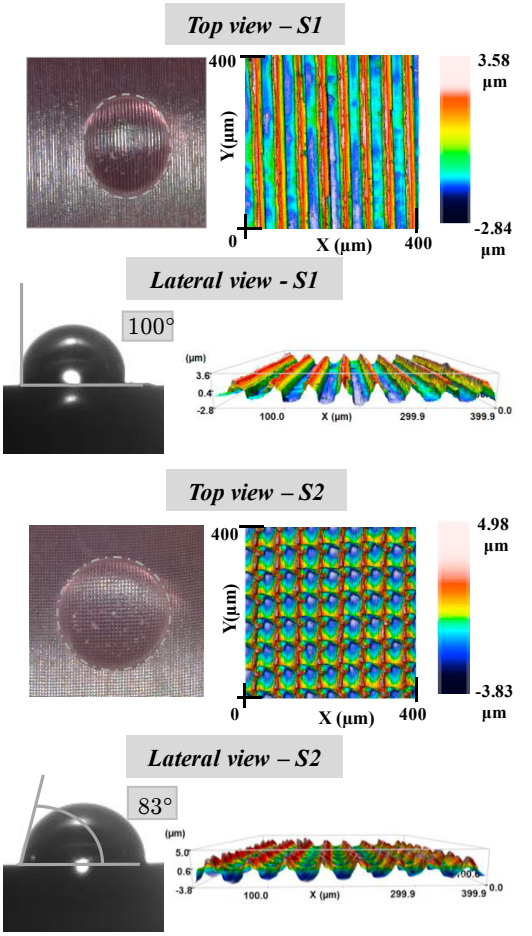

Fig. 8. Top and lateral view of the water droplets made to fall on the S1 and S2 samples. For sake of comprehension also the topographies relative to the different views are reported.

However, from the results reported in Section 3.1, no sensible differences were found between the mechanical properties of CT and UVT samples. Therefore, the surface energy does not play a role in this context.

The second factor is the surface topography. In particular, the creation of micro-textured surfaces can boost both hydrophilicity and hydrophobicity. In this case, the generation of a regular and well-determined pattern along the vibration direction contributed to increase wettability. However, such increase cannot be explained by the change in the surface texture parameters introduced in Section 3.2, since the considered surface texture parameters are demonstrated to be dependent only by process parameters other than the cutting approach.

Table 4 reports the measures of the contact angles of the UVT samples. As can be seen, no clear influence of the cutting speed and depth of cut can be highlighted. This can be ascribed to the fact that UVT introduces a texture perpendicular to the feed direction, but, for carrying out wettability measurements on cylindrical surfaces, the contact angles are measured parallel to the sample axis, and therefore the contribution of the UVT texture can be just slightly appreciated. This is clearly shown by the lateral topographies reported in Fig. 8, where it is evident that the feed, which was fixed for all samples, is the actual parameter conditioning the liquid droplets arrangement.

It is worth noting that contact angles measurements along the vibration direction were not possible to be carried out due to the cylindrical shape of the samples.

Table 4. Contact angles and standard deviations (see test ID in Table 1).

Test ID	S2	S4	S6	S8
Contact angle (°)	83	90	95	83
Std	2.4	1.8	1.4	1.9

3.5 *Coating characteristics*

Fig. 9 shows the images of the sample surface before and after coating. In the latter condition, the surface appears covered by a translucent “gel”. Nevertheless, the coating appears defects-free and homogeneous on the whole surface. The reported results are relative to sample S1, but similar outcomes were found for the other cutting conditions.

Fig. 10 shows the sections of the S1, S2 and S3 coated samples, while in Table 5 the measured coating thickness are reported. It is worth underlying that since in the case of CT the surface is un-textured along the vibration direction, only the S1 condition was analyzed and was taken as a reference for comparison with the other UVT samples.

From Fig. 10, it can be noticed the presence of small cracks and partial detachments that can be solely attributable to the polishing process in which hard particles are involved leading to the partial destruction of the softer interface.

As can be seen from the comparison between the S1, S2 and S4 samples, the introduction of a surface texture leads to a considerable increment of the thickness of the deposited coating. Actually, the coating thickness is equal to 6.3 µm in the case of CT, it increases of 35% in case of S2 and of 90% in the case of S4. This significant increase can be clearly attributed to the presence of a texture since dimples can act as puddles for the storing of the liquid solution.

Focusing on the effect of the UVT parameters, it can be seen that the thicker coating layer is obtained at the highest cutting speed, regardless of the adopted depth of cut.

At the highest cutting speed and lowest depth of cut (S4 sample), the dimples become less spread along the vibration direction, but, at the same time, they can store a higher amount of liquid solution (see Fig. 6).

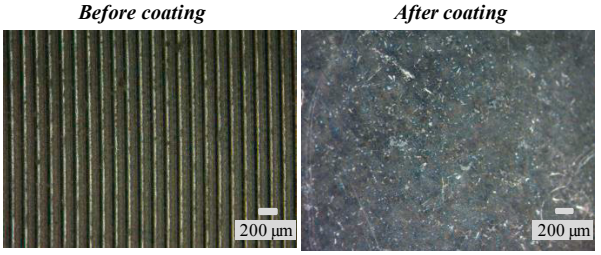

Fig. 9. Surface of the S1 sample after machining (on the left) and after sol-gel coating (on the right).

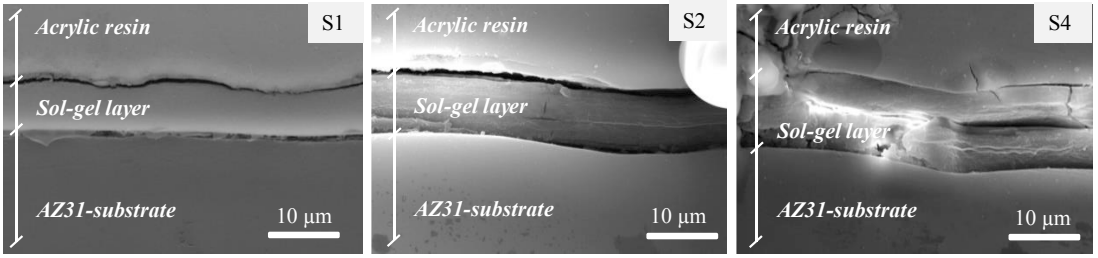

Fig. 10. Cross sections of the coated samples (see test ID in Table 1).

On the contrary, a moderate coating thickness increase is obtained in the case of the highest depth of cut (S6 and S8 samples), in the range of 6% and 10% compared to the S1 sample. Actually, a depth of cut increase leads to a sensible decrease of the dimples depth (see Table 3 and Fig. 6). Less deep dimples can store a lower amount of solution, leading, as a consequence, to a lower coating thickness.

The cutting speed effect is confirmed also at the highest depth of cut, namely the higher the cutting speed the thicker the coating, even if such enhancement is more restrained compared to what found at the lowest depth of cut.

Table 5. Measured coating thickness (see test ID in Table 1).

Test ID	Coating thickness (µm)
S1	6.3 ± 0.5
S2	8. 5± 0.2
S4	12.0 ± 0.4
S6	6.7 ± 0.2
S8	6.9 ± 0.4

4. Conclusions

In the present study, the effect of surface texturing as a method to prepare the surface for a subsequent deposition of a coating was evaluated.

Ultrasonic Vibration Turning (UVT) was exploited to create dimples on the surface of AZ31 magnesium alloy samples, varying both the cutting speed and the depth of cut in order to modify the arrangement of the dimples that covered the surface. Conventional Turned (CT) surfaces were produced as reference as well. Each machined sample was characterized in terms of mechanical, surface and wettability characteristics, before the application of a sol-gel coating.

The main results can be summarized as follows:

- UVT did not affect the AZ31 characteristics in terms of microstructure and nano-hardness, preserving the properties of the bulk material.
- A completely different surface texture was obtained when ultrasonic motion was applied to the cutting tool. Among the investigated cutting parameters, the depth of cut was the most effective in conditioning the *Sa*, *Spk* and *Svk* texture parameters.
- The cutting speed influenced the density of the dimples while the depth of cut noticeably affected their aspect ratio.
- UVT reduced the amount of surface defects generated on the machined surface compared to the CT case, contributing to the generation of a totally defects-free surface when mild cutting parameters were adopted.
- The texture surface induced by UVT contributed to increase the surface wettability of approximately 17% compared to the CT case, regardless of the adopted cutting parameters. In addition, the liquid droplets fallen on UVT textured surfaces were more isotropic thanks to the presence of a regular pattern orthogonal to the feed direction.
- The thickness of the deposited sol-gel coating was increased when applied to UVT surfaces, regardless of the adopted cutting parameters. However, the lowest depth of cut and highest cutting speed contributed to generate deeper dimples, and, therefore, increased the efficiency of the coating deposition.

In conclusion, it can be stated that UVT can represent an efficient method to machine magnesium alloys surfaces for biomedical applications that have to be later on coated for increasing their corrosion performances inside the human body, since UVT contributes to increase the efficiency of the coating deposition.

References

[1] Zheng, Y. F., Gu, X. N., Witte, F. Biodegradable metals. Mat Sci Eng: R 2014;77:1–34.

[2] Peron M, Torgersen J, Berto F. Mg and Its Alloys for Biomedical Applications: Exploring Corrosion and Its Interplay with Mechanical Failure. Metals 2017;7:252.

[3] Zhang E, Yang L, Xu J, Chen H. Microstructure, mechanical properties and bio-corrosion properties of Mg–Si(–Ca,Zn) alloy for biomedical application. Acta Biomaterialia 2010; 6:1756–1762.

[4] Bertolini R, Bruschi S, Ghiotti A, Pezzato L, Dabalà M. The Effect of Cooling Strategies and Machining Feed Rate on the Corrosion Behavior and Wettability of AZ31 Alloy for Biomedical Applications. Procedia CIRP 2017;65:7–12,

[5] Bertolini R, Bruschi S, Ghiotti A. Large Strain Extrusion Machining under Cryogenic Cooling to Enhance Corrosion Resistance of Magnesium Alloys for Biomedical Applications. Procedia Manuf 2018;26:217–227.

[6] Hornberger H, Virtanen S, Boccaccini AR. Biomedical coatings on magnesium alloys-A review. Acta Biomaterialia 2012;8/7:2442–2455.
[7] Rojaee R, Fathi M, Raeissi K. Controlling the degradation rate of AZ91 magnesium alloy via sol–gel derived nanostructured hydroxyapatite coating. Mat Sci Eng: R 2013;33:3817–3825.
[8] Guo P, Lu Y, Ehmann KF, Cao J. Generation of hierarchical micro-structures for anisotropic wetting by elliptical vibration cutting, CIRP Annals -Manuf Techno 2014; 63/1:553–556.
[9] Lu Y, Guo P, Pei P, Ehmann K.F. Experimental studies of wettability control on cylindrical surfaces by elliptical vibration texturing. Int J Adv Manuf Techno 2014;76/9–12:1807–1817.
[10] Liu X, Wu D, Zhang J. Fabrication of micro-textured surface using feed-direction ultrasonic vibration-assisted turning. Int J Adv Manuf Techno 2018;97/9-12:3849-3857.
[11] D Iorio E, Bertolini R, Bruschi S, Ghiotti A. Design and development of an ultrasonic vibration assisted turning system for machining bioabsorbable magnesium alloys. Procedia CIRP 2018;77:324-347.
[12] Bruschi S, Bertolini R, Ghiotti A, Savio E, Guo W, R. Shivpuri. Machining-induced surface transformations of magnesium alloys to enhance corrosion resistance in human-like environment. CIRP Annals-Manuf Techno 2018;67:579–582.
[13] Silberschmidta VV, Sameh M.A. Mahdyb. Gouda MA, Naseera A, Maurotto A, Roy A. Surface-roughness improvement in ultrasonically assisted turning. Procedia CIRP 2014;13:49-54.
[14] Zou P, Xu Y, He Y, Chen M, Wu H. Experimental Investigation of Ultrasonic Vibration Assisted Turning of 304 Austenitic Stainless Steel. Shock and Vibration 2015;2015.
[15] Xing D, Zhang J, Shen X, Zhao Y, Wang T. Tribological properties of ultrasonic vibration assisted milling aluminium alloy surfaces. Procedia CIRP 2013;6:539–544.
[16] Hosseinabadi HN, Sajjady SA, Amini S. Creating micro textured surfaces for the improvement of surface wettability through ultrasonic vibration assisted turning. Int J Adv Manuf Techno 2018;96:2825–2839.
[17] Amini S, Hosseinabadi HN, Sajjady SA. Experimental study on effect of micro textured surfaces generated by ultrasonic vibration assisted face turning on friction and wear performance. Appl Surf Sci 2016;390:633–648.
[